Journal of Electric Propulsion

RESEARCH

Open Access

High-resolution direct thrust characterization of electrospray thrusters with EMI-BF_4 at different temperatures and polarities

O. Neunzig[1*], P. Lozano[2] and M. Tajmar[1,3]

*Correspondence:
O. Neunzig
oliver.neunzig@tu-dresden.de
[1]Institute of Aerospace Engineering, Technische Universität Dresden, Marschnerstrasse 32, 01307 Dresden, Germany
[2]Department of Aeronautics and Astronautics, Massachusetts Institute of Technology, 02139 Cambridge, MA, United States of America
[3]Faculty of Space Technologies, AGH University of Krakow, Krakow, Poland

Abstract
Electrospray thrusters have garnered significant attention throughout the years as an exceptional propulsion technology for nano- and picosatellites due to their efficiency and precise thrust control. They operate on the principle of electrostatically accelerating charged particles (liquid droplets, pure ions or their mixtures) from ionic liquids and other low-volatility propellants, which are extracted from a Taylor-cone formation on top of porous emitter arrays. In this work we characterized the thrust performance of electrospray thrusters with the ionic liquid 1-ethyl-3-methylimidazoliumtetrafluoroborate (EMI-BF_4) as well as an attempt with an acetate-based ionic liquid. The arrays were operated at different polarities and at elevated temperatures of up to 43 °C which led to a decrease in viscosity and enhanced current emission for EMI-BF_4 with a factor of 1.43 at equal voltage levels. Temperature related effects resulted in a thrust difference of 3% between the maximum and minimum temperature throughout the tested current range. Thrust measurements for emission currents between 10 μA and 200 μA revealed a detectable and temperature independent difference between the positive and negative mode in favor of the negative polarity, indicating different ion-regimes compared to most data found in literature. The paper presents a novel thrust measurement setup for micro-propulsion systems based on a counterbalanced double pendulum thrust balance that achieves nanonewton resolution with the option to heat several thrusters. A comprehensive overview of the test setup and calculations of obtained electrospray parameters from experimental data is presented.

Keywords Electrospray, Thrust measurement, Ionic liquids, Electric propulsion

Introduction

Electrospray thrusters represent a cutting-edge propulsion technology particularly suited for small spacecraft applications such as CubeSats and nanosatellites. These thrusters capitalize on the electrostatic acceleration of charged particles in the form of liquid droplets in the jet-mode, ions in the pure ion-mode or their mixtures. Especially the pure ion-mode is of significant interest for such applications as it offers high efficiency and specific impulse that often exceeds a thousand seconds in conjunction with a miniaturizable, straightforward and reliable thruster module design. Furthermore, the ability to operate the device in both polarities eliminates the need for neutralizers.

As for any propulsion system, it has to undergo experimental validation of performance parameters in a laboratory environment such as beam divergence, long-term stability and especially thrust. Even though theoretical simulation models and methods to predict the performance of electrospray thrusters advance equally fast [1, 2], terrestrial tests are indispensable to verify each component and subsystem prior to in-orbit usage. Besides already mentioned parameters, thrust is the most important metric to experimentally validate as it enables the determination of a thruster's critical operating parameters. However, the expected thrust for an electrospray propulsion system in the range of only several micronewton opposes huge challenges towards the testing infrastructure, most notably, the thrust balance.

Experimentally acquiring thrust values for each operating mode allows to calculate specific impulse (I_{sp}), total efficiency and mass utilization amongst other fundamental characteristics of an EP-system. In general, electric propulsion generates thrust values on the order of several millinewton for concepts like Hall-effect thrusters or even micronewton for field emission electric propulsion (FEEP), which is comparable to electrospray thrusters. To measure these miniscule forces, thrust balances mechanically separate the thrust vector from the dominant gravitational force vector of a thruster's weight with different methods, most notably pendulums. Either in a hanging pendulum [3] or torsion pendulum configuration [4–6], pendulum-type thrust balances are able to detect forces with great accuracy [7]. But there are several effects and parasitic forces that easily influence balances and increase their noise. Among the most dominant influences are thermal loads, high-voltage and /-current, magnetic fields, connections from supply wires, rigid propellant tubes and much more. To filter the actual thrust value from these undesired influences, that are often much larger than the actual thrust, is a core requirement for experimental validations.

Several balances have been developed and optimized at the Dresden University of Technology (TUD) test facility. Our latest balances eliminate the majority of said influences, based on inverted counterbalanced double pendulums. This method was advanced to a level where even photon-momentum interactions in the range of nanonewton are detectable and we demonstrated this in previous publications with solar-sail applications [8–10]. This level of accuracy is well suited for thorough electrospray characterizations.

Electrospray thrusters underwent numerous direct and indirect thrust measurements with different ionic liquids in recent years by placing propulsion modules onto sensitive balances [11–20]. Krejci et al., for example, utilized a single electrospray thruster module with 480 single emitters and compared thrust measurements with two independent test facilities [11]. The comparison was done between a torsional thrust balance at NASA John H. Glenn Research Center [21] and a rotational thrust balance at the Massachusetts Institute of Technology (MIT) [12]. Both laboratories confirmed, that their measurements with EMI-BF_4 had a linear dependency between thrust and emitted current over the tested range of 20 μA up to 300 μA, which led to thrust values of up to ~ 23 μN. Both polarities were investigated with nearly equal force values for the torsion balance measurements. An additional measurement campaign with a torsional balance at the Propulsion Science Department at The Aerospace Corporation with MIT's scalable ion electrospray propulsion system (S-iEPS) consisting of several emitter arrays confirmed linear thrust dependency even for emission currents above 1 mA [14]. Mier-Hicks et al. developed the previously mentioned magnetically levitated testbed which allows for additional information regarding spacecraft charging. Here, thrusters operate in pairs of opposing polarity with EMI-BF_4 to neutralize the ion beam after acceleration and prevent backflow [12, 13].

Although the usage of thrust balances is preferred, another indirect method is applicable via time of flight (TOF) measurements. TOF measurement involve mass spectrometers to determine the mass distribution of different ion species in the emitted ion-beam. This method allows to identify and distinguish between singly-charged ions, droplets or whole clusters and may be used to estimate thrust and specific impulse without a thrust balance [11, 22]. We focused on direct measurements primarily, since it is more reliable and TOF data could not yet be acquired at the TUD test facility.

Guo et al. investigated thrust values of their ILET-3 device with EMI-BF_4 on a torsional thrust balance and compared the results of negative and positive polarities. They detected higher force values for the negative polarity compared to positive with direct measurements and via TOF data. This difference was attributed to different ion species in both regimes, leading to heavier cluster formation in the negative mode and, thus, increasing thrust due to a smaller charge-to-mass ratio [22].

While thrust and specific impulse have been studied intensively, a direct thrust performance evaluation at different temperatures is not found in literature, yet. For this exact purpose, we developed a dedicated measurement setup involving the double-pendulum type thrust balance with an on-board heating element and the capability to host several thruster modules on the balance simultaneously. We will present results on thrust performance for EMI-BF_4 at room temperature and with increased temperature as well as an attempt with a novel acetate-based ionic liquid, named EMI-Acetate (1-ethyl-3methylimidazolium trifluoroacetate). However, the latter opposed a critical handling difficulty due to an unexpected chemical incompatibility with the propellant storage unit. Consequently, results are focused on EMI-BF_4 primarily and will be extended to more ionic liquids in the future. The incentive for EMI-Acetate over EMI-BF_4 in electrospray thrusters originates from its enhanced wettability on electrodes, lower corrosivity and lower viscosity, which makes it more desirable for long-term missions, especially when corrosion is a concern. At first, we describe the function principle of the electrospray module developed at MIT and the test infrastructure at TUD. The following subsection is dedicated to the thrust balance and the calibration method which was employed for the tests. A section on thrust performance results for EMI-BF_4 at different polarities and temperatures conclude this work.

1. Electrospray thrusters

2.1 Function principle

At the core of electrospray thrusters is the phenomenon of electrospray emission, wherein a liquid propellant is exposed to a strong electric field, causing it to emit charged particles. This process begins with the formation of a Taylor cone at the tip of an emitter, typically pre-shaped by a fine needle or capillary [23]. When high-voltage is applied between the emitter and an extractor electrode, the liquid propellant forms a sharp, conical shape due to the electrostatic forces acting against the propellant's surface tension.

At the apex of the so-called Taylor cone with its characteristic half-angle of 49.3°, the electric field becomes sufficiently intense to eject charged droplets, ions or a mixture of both from the liquid surface. These emitted particles are then accelerated by the electric field, imparting momentum and generating thrust. Since thrust and specific impulse of colloid-type thrusters are proportional to the propellant's surface tension, changing the tension should have a measurable impact on thruster performance, as described by Lozano et al. [24]. Our goal is to decrease the surface tension during thruster operation by elevating its temperature within a vacuum environment to immediately detect behavioral changes in operating parameters and most importantly– thrust.

Typically, two operating regimes or a mixture of both (Fig. 1, B) are formed in electrospray propulsion - the cone-jet mode (Fig. 1, A) and the pure ion regime (Fig. 1, C). In the cone-jet mode, charged droplets are extracted from the tip of the Taylor cone by breaking the meniscus. The pure ion emission is accessed with electric field strengths at the emitter tip on the order of ~ 1 V/nm [25] in conjunction with ionic liquids as propellants. These liquids are molten salts with negligible vapor pressure, high electrical conductivity and they remain in the liquid phase at room temperature. They are composed of charges in both polarities, that can be extracted dependent on the applied emitter polarity. EMI-BF_4, for example, consists of the cation EMI^+ and the anion BF_4^-. Both of which possess different ion masses and, therefore, behave differently in terms of thrust sine q/m changes. However, operating the thruster in both polarities is necessary to neutralize the ion beam after acceleration, which allows the absence of a neutralizer. Additionally, the polarity alternation is required to remain chemical stability within the liquid and to prevent accumulation of only one charge, which could prevent further ion extraction and drastically shortens their life-time. However, the high electrical conductivity of ionic liquids and the fact, that single ions can be extracted and accelerated, increases the acquirable specific impulse significantly compared to the jet-mode.

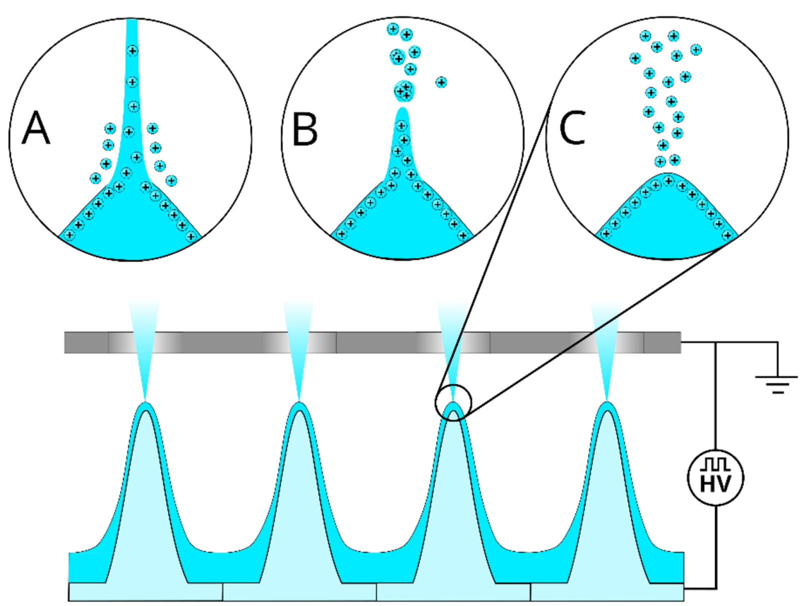

Fig. 1 Electrospray function principle with three exemplary operating modes. **A**: cone-jet mode with the formation of a narrow jet at the Taylor-cone's apex. **B**: Mixed mode with droplet formation. **C**: Pure ion mode by extracting single ions without breaking the meniscus. Example at positive polarity

The pure ion regime ideally has no jet-formation and its thrust is limited by the propellant flow-rate, amongst others, that can be transported to the emitter tips without entering the cone-jet mode. This allows a high thrust density and dense clustering in arrays. Such an array has been developed with the S-iEPS Electrospray system at MIT which will be further explained in the following subsection.

S-iEPS propulsion system

The MIT has been a pioneer in the development and refinement of electrospray thrusters, leveraging their unique characteristics to enhance space mission capabilities. At MIT´s Space Propulsion Laboratory, a highly miniaturized thruster that operates in the pure ion regime has been conceptualized, developed and tested successfully. One module is condensed into a thruster area of just 1 cm^2 with 480 single emitters that are arranged in a triangular pattern. Ionic liquid is fed to the emitter array passively through capillary forces from a layer of pyrolyzed carbon aerogel with high internal surface area [11, 13, 14]. The device features a storage tank made from polyetheretherketone (PEEK) that hosts enough propellant until the thruster's end of life (EOL).

For the tests presented in this work, we did not use the device at the finished product level. Instead, we tested the emitter-extractor array without the dedicated storage unit. The amount of stored propellant was therefore limited to around 85 mg through the available volume in the thruster's internal layers and the wetted emitters with a small portion that adhered to the back of the emitter array where the high-voltage electrode is attached. Two such devices were used for the tests that were aligned under a microscope and fixated to PEEK mountings. The entire measurement setup and its dedicated testing environment will be described in the following chapter.

Methods

Measurement environment

Tests were performed in our largest cylindrical vacuum chamber (Fig. 2). It has an inner diameter of 0.9 m, a length of 1.5 m and it is made from 304 stainless steel. A total of 4 windows (2 on each side, angled and non-angled) allow several camera angles and optical diagnostics. Two rails on the inside allow experiment setups on multiple layers,

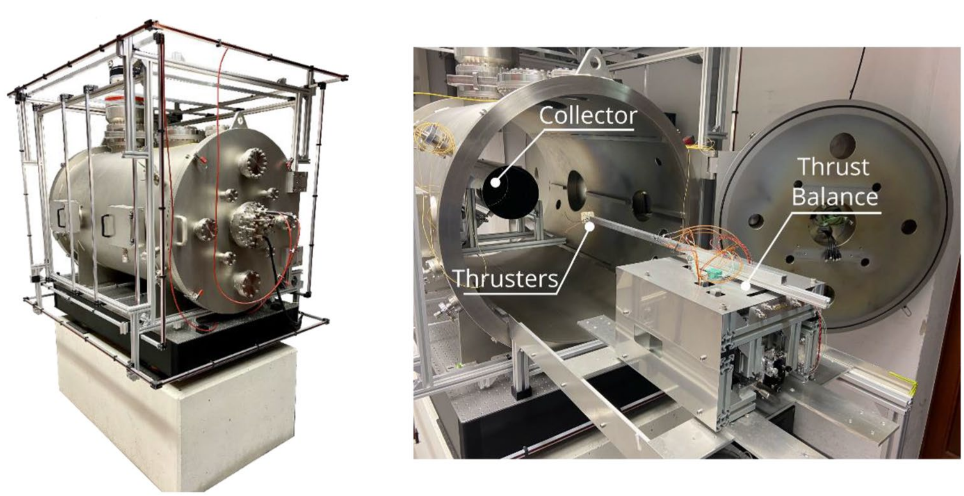

Fig. 2 Cylindrical vacuum chamber with an inner diameter of 0.9 m, a length of 1.5 m, an Edwards XDS35i first-stage scroll pump and a Pfeiffer Hipace2300U second-stage turbomolecular pump

which is used for the measurement setup. The first-stage pump is an *Edwards XDS35i* scroll pump that creates a rough vacuum of $3 \cdot 10^{-2}$ mbar. The second stage pump is a *Pfeiffer HiPace2300U* turbomolecular pump. During measurements the base pressure reached $3 \cdot 10^{-7}$ mbar. Unlike our biggest rectangular chamber used for thrust measurements with high gas-loads [26–28], the cylindrical chamber does feature seismic isolation and a dedicated Helmholtz coil array. By positioning the chamber on a concrete block, that is decoupled from the building, seismic noise is decreased from measurements that require very high resolution. Although the concrete block eliminates a lot of seismic excitations from the lab-building, traffic from roads nearby and people walking in the lab still disturb sub-μN measurements, hence, measurements are done primarily during decreased seismic activity throughout the night. On top of the concrete block sits an optical table to level the chamber. Each window is optically sealed for laser experiments and photon propulsion measurements [8–11].

The cuboid coil array allows dedicated magnetic field topologies via four concentric coils that create magnetic flux along the cylinder's symmetry axis and four additional coils for the remaining two axes, two from each side. The array enables a large volume within the chamber with distinct magnetic fields or even cancel Earth's magnetic field, since it's a driving factor in systematic thrust measurement errors due to the formation of Lorentz forces in conjunction with electrical currents on a thrust balance.

Thrust balance development

Since the propulsion system ejects charged particles and possibly droplets of electrically conductive propellant, we utilized our compact thrust balance (CTB) that is shielded against plasma interactions with sensitive components. Its measurement principle is based on an inverted counterbalanced double pendulum and it is the second generation double-pendulum balance besides our nanonewton thrust balance (NTB) [8–10].

Both balances obey the same measurement principle which is based on a spring-loaded parallelogram onto which a thruster applies a linear force (Fig. 3). The propulsion system is situated on a dedicated platform and its mass is counterbalanced with optional counterweights. The thruster platform is connected to three rigid pendulum arms to support and distribute the load on up to six bearings. These bearings are frictionless flexural springs that create a restoring torque to any thrust from the propulsion system. An *attocube IDS3010* laser interferometer detects deflections of the pendulums once a force is present. To gain the actual force value, the deflective behavior is characterized with an integrated voice coil calibration system. The voice coil actuator (VCA) creates linear magnetic forces from sub-nanonewton to tens of millinewton with a *Keithley 2850* current source.

By deliberate center of mass (COM) shifts, a fraction of the thruster's gravitational force is introduced as another counteracting force. to access a broad bandwidth of measurement ranges. High resolution is acquired at the cost of reaction time and vice versa.

Detailed properties of the balance and its measurement principle are presented in Fig. 3; Table 1. Our balances were designed for nanonewton resolution with thruster masses of up to 10 kg and a measurement range of 1 mN. In previous publications we could prove, that they are able to detect the force generated by a steady-state laser with 0.5 W of power– which corresponds to less than 1.7 nN [10]. The NTB is mainly used for photon propulsion applications and propulsion systems with self-sufficient propellant

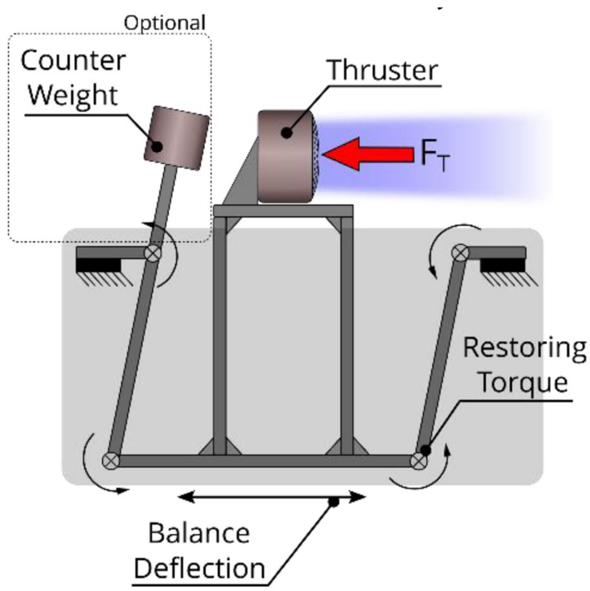

Fig. 3 Thrust measurements principle of the compact thrust balance (CTB) based on a non-inverted double pendulum. Linear forces from propulsion systems lead to a deflection of the spring-loaded parallelogram which is measured by an interferometer

Table 1 Thrust balance specifications

	Value
Balance Dimensions	(400 × 360 × 300) mm^3
Net weight, approx.	18 kg
Maximum load	10 kg (< 5 kg for highest resolution)
Measurement range	Up to 50 mN
Resolution	Sub-µN below 10 kg (nN at 5 kg and less)
Average response time (load dependent)	3–15 s
Electrical connections	5 x High-voltage (10 kV) 6 x Low-voltage (0.5 kV)
Thermocouples	1–5
Propellant tubes	2

storage like electrospray thrusters and whole CubeSats. Up to 20 electrical contacts supply propulsion systems with 1 A / 50 V each or serve as connections for thermocouples and serial- or WiFi communication.

The CTB is a more compact balance that inherited the best features from experience with the NTB. It is utilized to characterize all kinds of plasma thrusters ranging from HETs to FEEP, Electrospray thrusters and even cold-gas systems. It supports thruster loads of 10 kg with sub-µN resolution or loads of 5 kg with nanonewton resolution for measurement ranges of up to 50 mN. Six low-voltage contacts (500 V/1 A) and five coaxial high-voltage connectors (10 kV/3 A) together with three thermocouples complete the electrical interface (Fig. 4). The electrical contacts and all sensitive components are encased in a stainless-steel housing to increase resilience to plasma interactions. Two propellant tubes offer continuous gas-supply, both of which were dismounted for the electrospray measurements. The balance utilizes specially shaped liquid metal connectors to neglect stiffness from wires from the measurement and they allow continuous current and voltage supply from outside the vacuum chamber for long-duration testing.

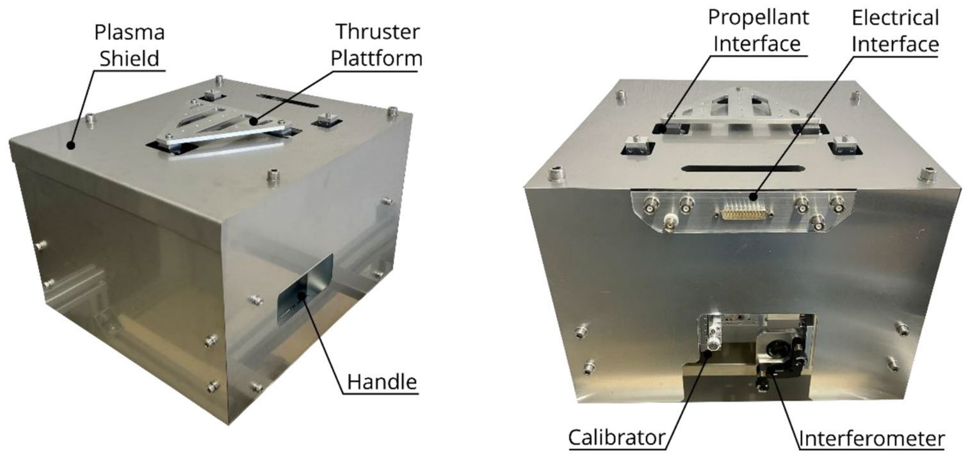

Fig. 4 Left: Balance front with a stainless-steel plasma shield, handles and the thruster platform. Right: Rear side of the CTB with access to the voice coil calibrator, the interferometer lens and the propellant- as well as its electrical interface with five high-voltage MHV connectors and a D-Sub 25 connector

In general, the double-pendulum principle has several advantages over state-of-the-art torsional balances, which are the most common type. Heat generation from propulsion systems on the balance inevitably change the center of mass (COM) of the thruster. Torsional balances are quite sensitive to these COM-movements as they lead to a deflection of the balance, which is then misinterpreted as thrust. The static determinacy and weight distribution on three columns in double-pendulum-type balances drastically decrease this measurement error, as shown in previous publications [29]. Furthermore, torsion balances need the propulsion system to be placed on one end of their lever arms while a counterweight is placed on the other lever arm with the same length. This is necessary to not damage the bearings from lateral forces due to high torques. Especially small vacuum chambers face this issue as the thruster must be positioned off-center and often very close to the chamber wall. Ideally, thrusters are positioned in the center of the chamber to allow an evenly distributed plasma plume for external beam diagnostics. Additionally, with torsional balances the exact lever arm length between the thrust vector and the bearings must be determined each time for thrust calculation, which increases error calculations.

Double-pendulums can be built in a nested configuration and, thus, very compact to position the thruster always in the center of a vacuum chamber. Lever arms are always the same independent of thruster position, because the actual pendulum mechanism only reacts to forces that are transferred from the thruster platform where they originate from (Fig. 4, left). Any distance from the thrust vector relative to the platform is irrelevant for the measurement as long as the thruster is fixated to the platform. This means, that these balances are very versatile in its installation and thruster position.

The CTB may be used either in direct or indirect measurement applications. Direct thrust measurements are straight forward and reliable, wherein a propulsion system is placed on a thrust balance and it is supplied with electrical power and propellant through the balance´s interface. Any electronics and propellant storage units are outside of the vacuum chamber. The entire impulse generated by the thruster is transferred to the test stand and converted to time-dependent thrust values. Balance interfaces are designed to not alter the thruster's operating parameters so that the thruster should not be able to tell the difference between operation fixated in a vacuum chamber, in outer space or positioned on a thrust balance. While this is the case for most DC-systems like electrospray thrusters, it is quite the opposite for systems that operate on high-frequency ionization like radiofrequency ion thruster (RIT), for example. For this case we developed a non-invasive indirect measurement method. In a previous publication we showed, that indirect measurements of a Hall-effect thruster are as reliable as direct measurements by using a titanium collector on the balance while the propulsion system targets the collector from a fixed position in front of the balance [26]. For the electrospray thrust measurements, we used the direct method solely.

Thrust balance calibration

In this section we will present the calibration process and characterize the measurement environment. Prior to and after each test the balance is calibrated with an integrated VCA. This ensures unaltered balance performance throughout the test campaign and confidence in obtained thrust values. Depending on the thruster and desired measurement range, the sensitivity may be changed with counterweights.

In general, a calibration is performed by applying defined forces with the voice coil to measure the resulting balance deflection. An example is provided in Fig. 5 (A), where forces between ± 15 mN in steps of 2 mN are generated. Forces are generated for 40 s each and compared against the base value. The individual balance deflection-response is measured by the laser interferometer and plotted against the commanded forces to gain data points for each value. Ideally, these consecutive data points follow a linear trend that is fitted to them in Fig. 5 (C). Outcome of this process is the so-called calibration-factor K in the units [µN/µm] or [mN/µm] which is the gradient of the linear fit and represents the balance´s sensitivity. In the case of Fig. 5 (A, C) the balance was set to a high measurement range with a K-factor of 0.148 mN/µm and a standard deviation of

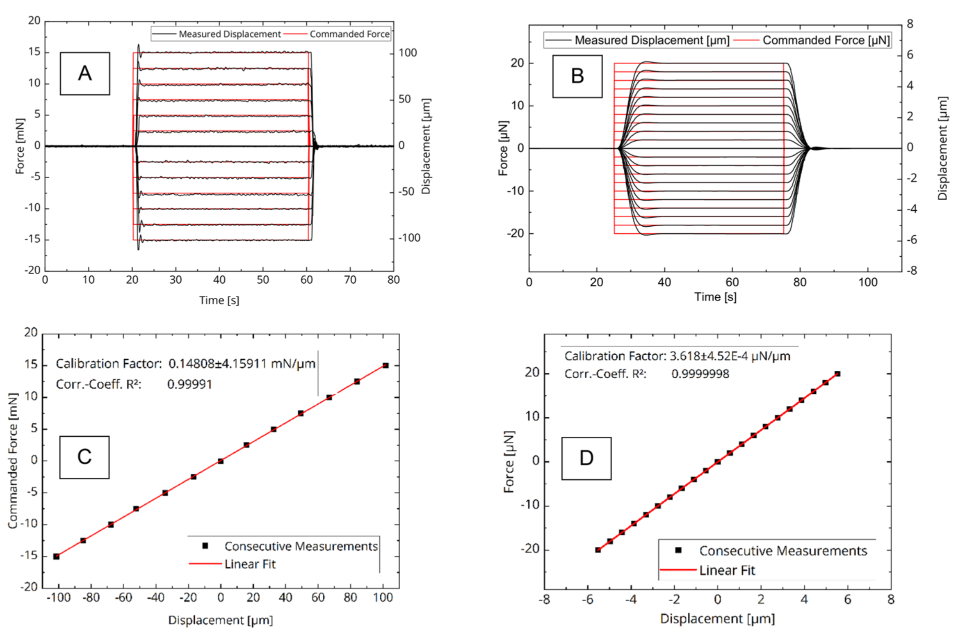

Fig. 5 Calibration results for two different measurement ranges and calibration factors. (**A**) Applied forces against measured displacements for forces from ± 15 mN in steps of 2.5 mN. (**B**) Applied forces of ± 20 µN in steps pf 2 µN. (**C**)-(**D**): Linear fit through the consecutive data points gained from (**A**)-(**B**) to acquire the calibration-factor

0.00042 mN/μm. Another example is provided in Fig. 5 (B) and (D) where the balance is set to high resolution. By applying forces of ± 20 μN in steps of 2 μN, the rcalibration factor resulted in 3.62 μN/μm with a standard deviation of 0.0046 μN/μm. Directly comparing the two cases (A) and (B) illustrates the trade-off in balance response time when the resolution is increased. During measurements, the K-factor is used to directly calculate the force from monitored deflections.

When mounting the propulsion system, a coarse calibration is performed at atmosphere to approximate and adjust the K-factor if necessary. Once at a vacuum environment, a more detailed calibration with decreased step-sizes is performed shortly before and after the actual thrust measurements.

To gain noise values for the electrospray measurements, the balance was operated at high-resolution settings and exposed to its measurement environment. There are countless effects that may affect thrust measurements. The most important influences are seismic noise, electromagnetic- and thermal interactions. Especially seismic noise from vacuum pumps can be challenging to eliminate, therefore, the natural frequency of the balance was set to values far lower than the influential frequencies from the turbopump and the scroll pump to neglect their impact on thrust measurements.

The electrospray characterization with the CTB in the following chapter was performed at high-resolution settings between 1.8 μN/μm and 4 μN/μm. Different sensitivities were used to utilize the faster balance response at high K-factors to investigate thrust instabilities. On average, the balance noise throughout the testing campaign was below 2 nN with an exemplary comparison of commanded forces vs. measured forces in Fig. 6 close to the balance resolution at nanonewton level. Note, that the y-axis unit changed from μN to nN. Here, we subsequently commanded forces between ± 10 nN, ± 5 nN and 0 nN and the noise value resulted in (0.01 ± 0.13) nN, (value ± StDev.), which leads to a signal to noise ratio of around 40 even at nanonewton range.

Measurement setup and thruster integration

Thruster integration involved two emitter arrays mounted close to another on the thrust balance, defined as *Thruster A* and *Thruster B* (Fig. 7, left). This way, the arrays could be loaded with different propellants and operated either as a stand-alone thruster, in pairs or alternating. The goal was to investigate several operational modes between the well characterized EMI-BF_4, hosted by *Thruster B*, and the novel EMI-Acetate, hosted by *Thruster A*. Figure 7 (left) shows the mounted thrusters next to each other on PEEK

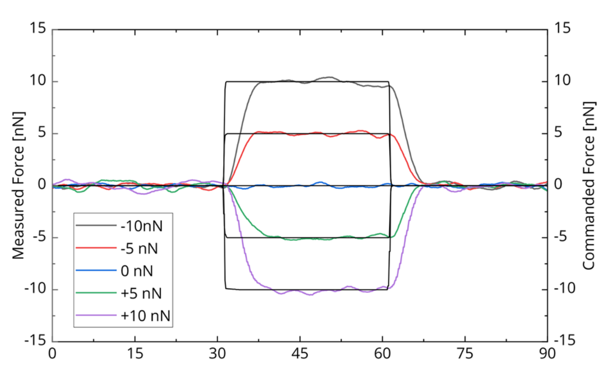

Fig. 6 Comparison of commanded vs. measured forces close to the balance resolution at nanonewton level

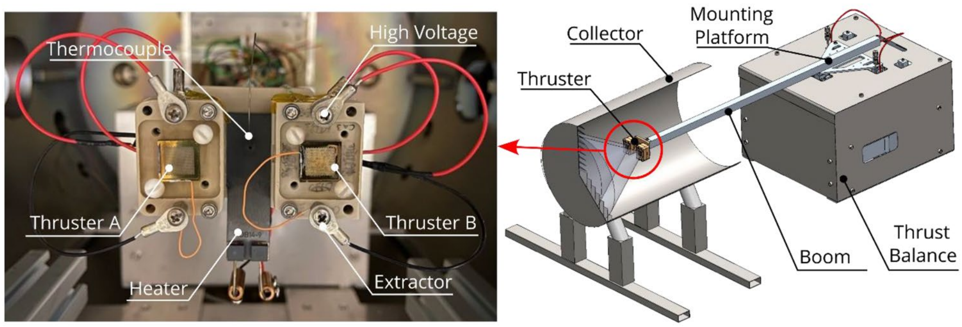

Fig. 7 Left: Two thrust devices mounted to the balance that are pressed against a ceramic heating element. Right: Measurement setup with the thruster and heater mounted to the tip of a mechanical boom, which is fixated to the thrust balance's platform. Wires and additional connections lead through the boom and both thrusters are inserted into a stainless-steel collector

housings and connected to the high-voltage supply wires as well as the grounded extractor grids. A ceramics heating element was pressed against the backside of each thruster for enhanced thermal conductivity. As described in previous chapters, the influence of temperature on thruster performance should be investigated, hence, the heater was connected via a sheathed thermocouple at the center of the heating element and two standard K-thermocouple wires close to each emitter array to observe the important temperatures.

Figure 7 (right) illustrates the entire measurements setup, that is positioned in the vacuum chamber. The shielded thrust balance is situated on the right side with a mechanical boom fixated to the thruster mounting platform. As described in the previous chapter, the double pendulum measurement principle allows the thrust vector to be anywhere in the chamber as long as it is rigidly connected to the mounting platform. Due to this feature, we decided to get a sufficient amount of distance between the balance and the emitters to further protect the balance and sensitive optical components like the interferometer lens from ejected ionic liquids. At the tip of the mechanical boom the previously mentioned thrust devices in conjunction with the heating element are mounted and inserted into a stainless-steel collector. The collector is not in direct contact with the balance setup, instead, it is mounted to rails that are fixated in the vacuum chamber. Situated at the bottom of the collector, there are several fins with a characteristic inbound bent shape to suppress back sputtering as good as possible and trap the majority of charged and neutral particles ejected by the thrusters. Both thrusters maintained a distance of 200 mm to the collector's fins. The entire collector is floating with respect to the chamber ground due to PTFE isolators. This way, the collector is connected to a current measurement device to gain values for the total emitted current. Furthermore, the collector may be charged to a bias voltage of up to 20 V to trap secondary species from facility related interactions mainly due to the impacting ion beam onto the collector surface. This is done to prevent backflow to the thrusters, which was investigated in literature [30–33] and leads to current imbalances between the emitter current in direct comparison to the extractor and collector currents. The collector current was mapped by a *Keithley 2450* current source whilst both extractor grid currents were measured via shunt-resistors. Alternating polarities on the thruster were applied by two *FUG HCP 35-20000* high voltage power supplies with integrated polarity switches.

All connecting wires were fed from the thrusters through the mechanical balance boom and connected via the balance's electrical interface to the data acquisition and power supplies on the outside of the vacuum chamber. The entire setup is illustrated in Fig. 8 within the cylindrical vacuum chamber.

To operate the entire measurement setup, we used the following devices outside the vacuum chamber. Each device was connected through the balance's electrical and propellant interfaces:

Devices - Balance operation:

- *attocube IDS 3010* laser interferometer for distance measurements.
- *Keithley 2450* current source for the voice coil calibrator.
- Three K-thermocouples at selected positions around the balance, connected to a *LabJack T7*.

Devices - Thruster operation:

- Propellants: EMI-BF_4, EMI-Acetate.
- Two *FUG HCP 35-20000* high-voltage power supplies with integrated polarity switches.
- *Keithley 2450* current source to measure collector (emitted) currents.
- Two shunt resistors to measure extractor (intercepted) currents with a self-developed data acquisition board.
- Two K-thermocouples close to each emitter array.

Devices– Heater operation:

- ceramics heating element.
- *EA-PS 5400* power supply for heater power.
- One sheathed K-thermocouple at the heater's core temperature.

Devices– Diagnostics:

- *Sartorius AX224* balance to obtain propellant consumption through mass changes before and after thrust measurements.

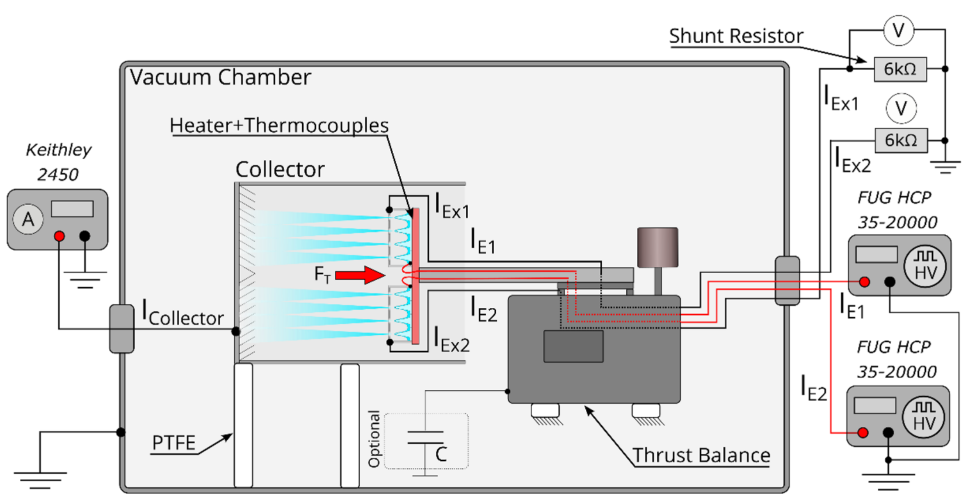

Fig. 8 Illustration of the measurement setup including electrical interfaces and devices

All devices, vacuum pumps and data acquisition were controlled by a LabView-based software with a dedicated script language.

To get a better understanding on temperature distribution on the emitter arrays, we added a *FLIR* thermal camera to the setup, electrically isolated, and positioned within the collector (Fig. 9, A). The thermal camera does not allow the determination of temperature, but it gives a qualitative image of the heat distribution, complemented by the three thermocouples. As seen in the comparison between Fig. 9 (B) and (C), the PEEK mountings of both arrays led to a decreased thermal conductivity. Because of this, the heater had to operate at temperatures above 100 °C for several hours to gain 43 °C at the emitter positions, which was the practical limit at this point. As a next step for additional measurements, we will incorporate increased thermal conductivity with electrically isolated thermal conduction paths.

Measurement results

EMI-BF_4

The entire measurement campaign was dissected into three sets of thrust measurements. Each of which started and ended with a mass determination of the devices with a *Sartorius AX224* balance with a resolution of 0.1 mg, allowing specific impulse calculations. However, it is important to mention that the devices were not operated at one specific emission current, but a multitude of currents to investigate thrust dependency on current. Therefore, specific impulse and charge-to-mass calculations were averaged over the entire current range of 10 μA-240 μA. This of course leads to variations from the actual specific impulse at each current level due to possibly different operating regimes, but we focused on thrust characterization primarily.

The first thruster was operated with EMI-BF_4 solely without the second device initially. We chose to test the well-characterized ionic liquid at room temperature first to compare the results to previous measurements at different independent laboratories. This ensures equal behavior of the array before investigating the influence of temperature.

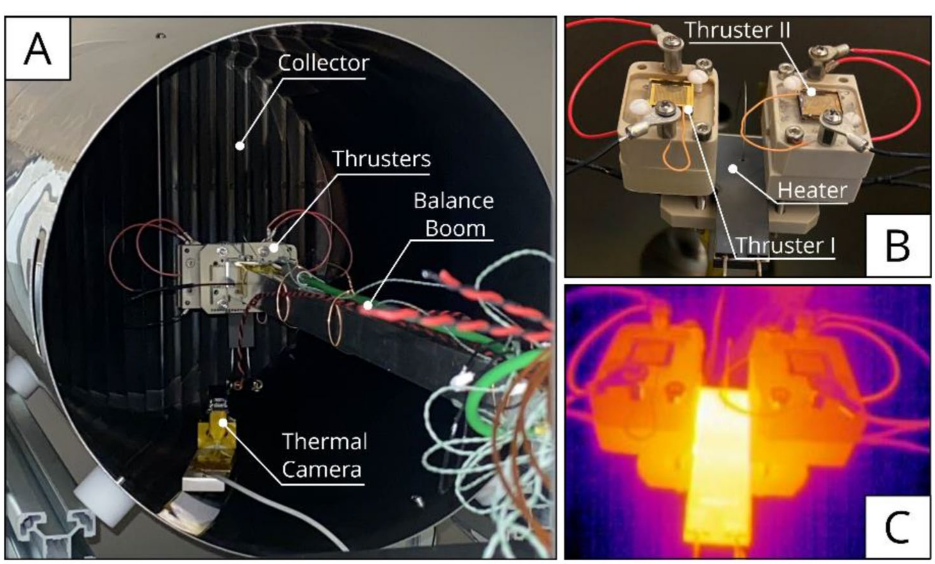

Fig. 9 (**A**): Details of the boom's end with the rear side of both thrusters inside the collector and a thermal camera oriented in an angle to prevent lens obstructions by the ionic liquid. (**B**)-(**C**): Field of view of the thermal camera

Prior to thrust measurements, the thruster's operating parameters were determined via a voltage sweep in both polarities. Figure 10 (left) illustrates this sweep with a quick voltage increase from 0 V to 700 V, as the thruster was expected to start emission at higher voltages. The following voltage levels between 700 V and 950 V were swept more slowly in a time frame of 200 s while observing the power supply unit (PSU) parameters as well as collector- and extractor currents. The collector- and extractor currents are often referred to as emitted- and intercepted current respectively.

At approximately 740 V emission of positive charges began and increased discontinuously to the chosen maximum current of 300 µA at 950 V. From the current signature it is obvious that, starting at around 70 µA, the intercepted current increased drastically, leading to an intercepted current of 75 µA at 300 µA of PSU current. Such a large intercepted fraction of ~25% is atypical compared to data found in literature [11–13]. It may indicate a slight misalignment of the emitter array and the extractor grid which would increase intercepted currents. This may be attributed to the fact, that it was the first thruster assembled and aligned at TUD laboratories. Nonetheless, the thruster was functional and used for this measurement campaign. The negative polarity sweep in Fig. 10 (right) indicates similar behavior regarding intercepted current. Here, the extractor intercepted a current fraction of ~18% at 300 µA, which is considerably less than the positive polarity, but still atypically high for the devices. But the current signature from the start of emission until the maximum current of 300 µA exceeds a more continuous increase at negative polarity.

Thrust measurements are performed in a distinct manner. By operating the thruster for several times at equal operating parameters, we increase statistical significance of the obtained thrust values. Especially for the lower current levels below 50 µA, four such measurements were averaged. Each time the thruster operated for 30 s with an on-/off delay of 30 s to gain a zero-reference for the thrust value. An example is provided in Fig. 11 (up) with a commanded current of 120 µA starting with positive polarity and switching to negative polarity for the following thrust value in an alternating manner. Here, the thrust signatures follow an ideal rectangular thrust balance response. However, in the very low current range (Fig. 11, down) the negative polarity does not entirely reach steady-state operation within the given time. Instead, the thrust decreases marginally over time despite a constant emission current, which may hint at a slight deviation at such small emission currents from the thruster's typical behavior, which is only seen with high thrust resolution. The positive polarity, on the other hand, exerts a much more stable thrust with almost no variation below emission currents of 10 µA. Furthermore,

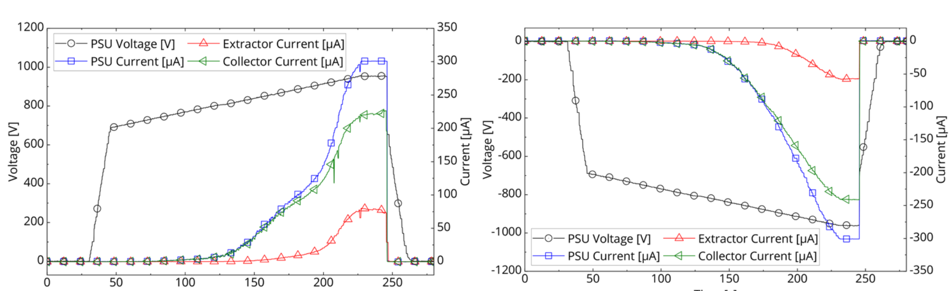

Fig. 10 Left: Gradual voltage sweep at positive polarity with EMI-BF_4 while observing emitted and intercepted current with a maximum current allowance of 300 µA. Right: Gradual voltage sweep at negative polarity in the same manner

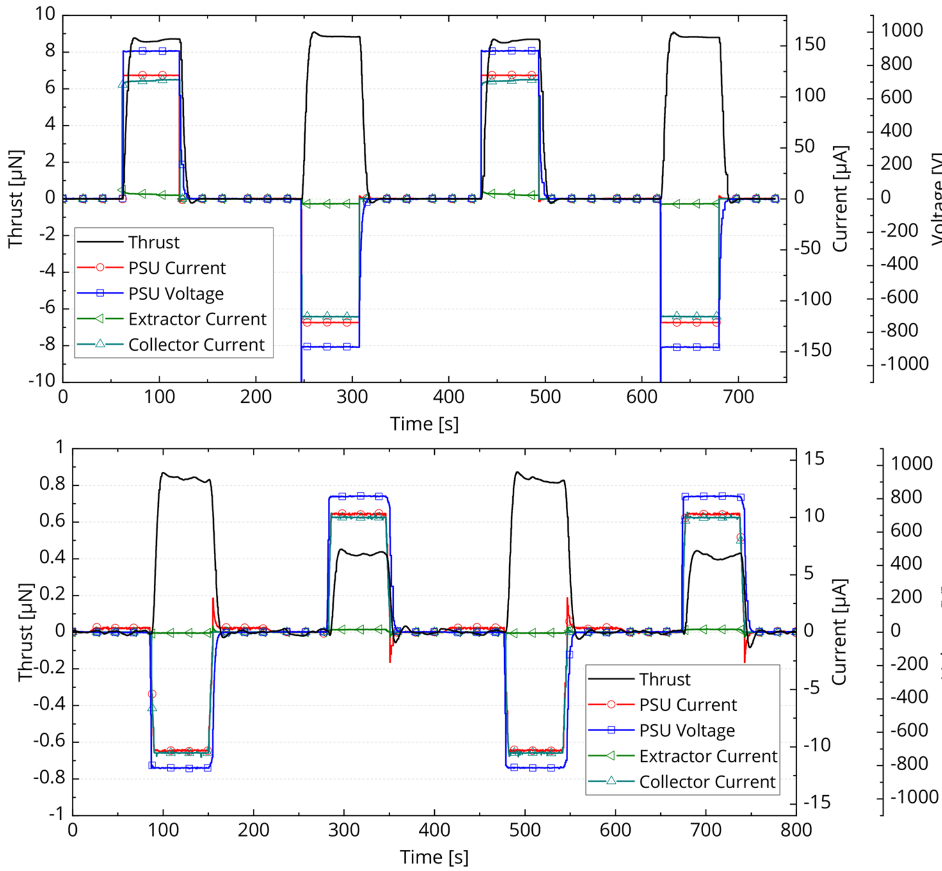

Fig. 11 Up: Four thrust measurements at equal operating parameters, but alternating high-voltage polarity for an emission current of 120 µA. Down: Subsequent thrust measurements at lowest emission current of 10 µA at alternating polarity

the negative polarity provides slightly more thrust than the positive polarity. This was unexpected as thrust values found in literature indicate, that the thrust for both polarities are close to another, but with a bit higher result at positive polarity. In fact, the ionic constituents of EMI-BF_4, which are the cation EMI^+ and anion $BF4^-$, do have different masses of 111 g/mol and 87 g/mol respectively [24, 34]. In the pure ion regime, we would therefore expect higher thrust for the positive polarity since q/m decreases. Considering the thrust data at very low emission currents with an example in Fig. 11 (down) at 10 µA, we see this effect even increasing. Here, obtained thrust values are almost halved for the positive polarity compared to negative.

Figure 12 summarizes thrust data over the entire current range. Note, that the x-axis only shows the collector current, which is the emitted current, and does not depict the extractor losses. The data shows a linear dependency between thrust and emitter current, which is consistent with data from different laboratories. Krejci et al. obtained 11 µN-12.5 µN at emission currents of 150 µA [11], which is in line with the 10.5 µN at 140 µA in our measurements at room temperature. However, the thrust difference between positive and negative polarity remains although they tend to equalize for emission currents upwards of 100 µA. We assume that this is due to an operating regime, that deviates slightly from the pure ion regime (PIR). At negative polarity, larger ion clusters might be present, especially at low emission currents. Such a cluster formation

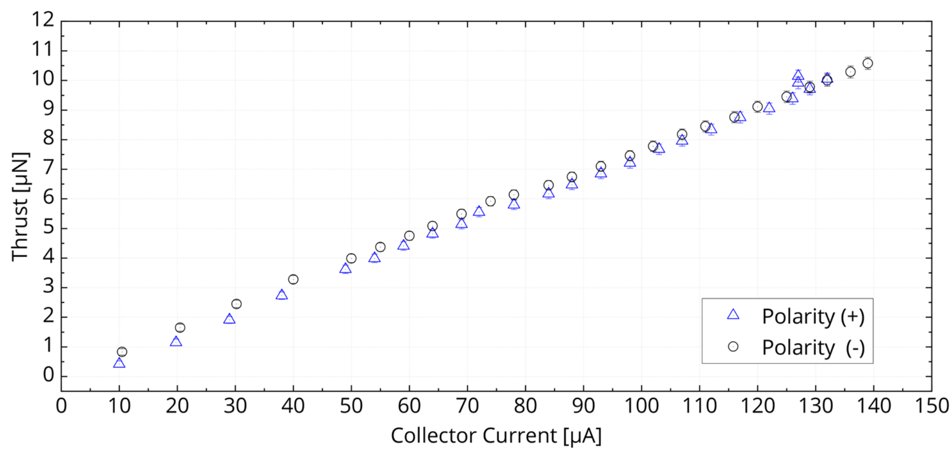

Fig. 12 Summary of thrust measurements with collector (emitted) currents of 10 µA to 160µA in positive and negative polarity. Each data point represents an average of 1–4 single measurements to increase statistical significance

was observed by Guo et al. during the investigation of their ILET-3 device on a torsional thrust balance [22]. They compared thrust results between negative and positive polarities and detected higher force values for the negative polarity compared to positive with direct measurements and via TOF data. This difference was attributed to different ion species in both regimes, leading to heavier cluster formation in the negative mode and, thus, increasing thrust by a smaller charge-to-mass ratio. Another explanation involves the likely misalignment of emitter and extractor, which was indicated by large intercepted currents previously. Additionally, the close distance to the collector might have played a role in this behavior, but it is speculative at this point and requires further investigation. Such facility effects may be a main contributor to this phenomenon, since the emergence of secondary species upon beam impact at the collector surface interact with electrospray plumes. Uchizono et al. investigated related phenomena and reported emission characteristic altering effects alongside mitigation strategies [30]. Additional publications by Klostermann et al. [31] and Hofheins et al. [32] provide experimental data for the creation of not just secondary electrons, but ions at beam impact on different surfaces, that are influenced by collector bias voltages and surface materials as well as surface textures of the collector. Since the collector in our setup is close to the emitters, such effects are likely and will be taken into account for an improved setup with a collector that surrounds the entire thrust balance. These implications of possible current imbalances from literature between emitter, extractor and collector current from the creation of secondary species were investigated with the underlying current data from Fig. 12. The imbalance was calculated via Eq. (1), that represents a current ratio between the sum of current fractions ($I_{Extractor}$+$I_{Collector}$), that are measured via shunt resistors and the Keithley 2450 respectively, and the total output current from the driving power supply to the emitter arrays ($I_{Emitter}$) in percentage.

$$\begin{aligned} CurrentRatio\,[\%] &= \left[1 - \frac{CurrentFractions}{EmitterCurrent}\right] \cdot 100 \\ &= \left[1 - \frac{I_{Extractor} + I_{Collector}}{I_{Emitter}}\right] \cdot 100 \end{aligned} \tag{1}$$

Ideally, this ratio results in 0%, which means that there are no imbalances from the creation and interaction with secondary species and no current measurement errors are present. The results are shown in Fig. 13 for negative and positive polarity with a direct comparison of current imbalances at + 20 V collector bias and without a bias voltage. Evidently, the current imbalance is close to zero with some fluctuations, that are mainly driven from the uncertainty of the FUG HCP 35-20000 power-supply at such small currents. Furthermore, the collector bias did not have a significant impact on current imbalances, which is a good indicator for the chosen collector design with slanted fins, that traps the majority of emitted currents and secondary species. However, the absolute collector and extractor current fractions are different between positive and negative polarity for equal emitter currents, as already discussed in Fig. 10.

Nonetheless, if we take the exemplary measurement of (8.32 ± 0.27) μN from Fig. 12 for a commanded current of 100 μA and assume an equal force distribution across all 480 single emitters of the array, we get a force of 0.017 μN or 17 nN per emitter. Considering the sub-nN resolution of the balance at highest accuracy settings, described in subsection 3.3, even single emitters could be characterized with our measurement setup.

As previously mentioned, specific impulse calculations took place by determining the mass loss of each thruster during a measurement session by comparing weights before mounting the thruster to the balance and after venting the chamber. Since ionic liquids have an inherent affinity towards water and humidity, we immediately measured its weight after tests once the chamber was vented and kept it stored in a desiccator while not in use.

Two methods may be used to calculate the I_{sp}– an idealized, indirect method and a direct method. The indirect method according to Eq. (2) overestimates the real specific impulse as it assumes loss-free operation. Here, the determination of q/m was done experimentally and emitter voltages $U_{Emitter}$ were used at different potentials. It is important to mention, that these calculations are all averaged over the entire current range instead of a single localized current and voltage level. Using this assumption, the calculated I_{sp} will not be applicable to distinct emission states. The same case applies to the second method according to Eq. (4) with a direct calculation of specific impulse from the total thruster operation time $\Delta t_{operation}$ and total mass loss $\Delta m_{EMI\text{-}BF4}$.

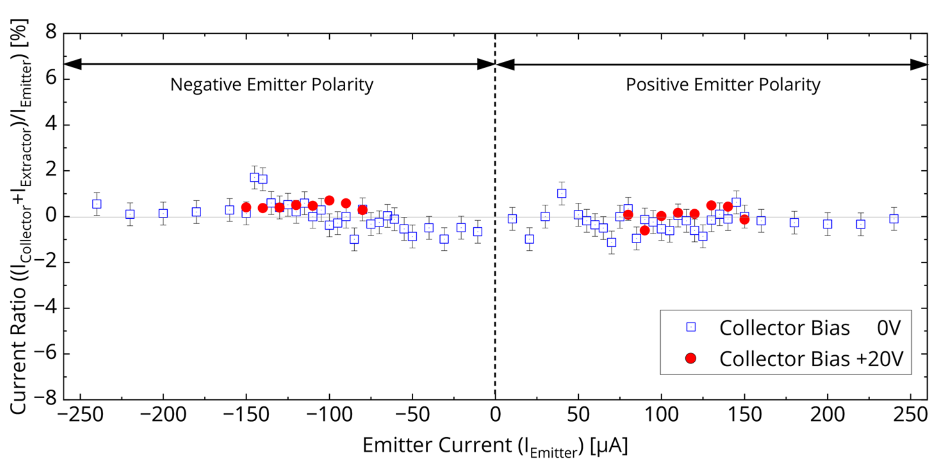

Fig. 13 Influence of collector bias voltage on emitter-, extractor- and collector currents at negative and positive emitter polarity

For the calculations, we used the underlying data from Fig. 12. Here, the devices operated at different current levels and voltage sweeps were performed as described in Fig. 10. This meant, that an integration of current over time was necessary for the entire set of data points, which resulted in an operating time of 110 min. The mass-comparison before and after this test resulted in a propellant consumption of 8.6 mg. Since it was a short-time test, the mass-change is very low and close to the balance resolution, which increases error calculations for the specific impulse. The total ejected charge accumulated to 0.5064 C, which leads to a charge to mass ratio of $5.89 \cdot 10^4$ C/kg or 58.9 C/g for EMI-BF_4. Krejci et al. determined a charge to mass ration of 72.5 C/g with this method, which is 18.7% higher than our results [11]. With this value we calculate the averaged ideal specific impulse to 1044 s according to Eq. (2).

$$I_{sp,ideal}^{average} = \frac{1}{g_0}\sqrt{2U_{Emitter}\frac{q}{m}} \tag{2}$$

$$\dot{m}_{average} = \frac{\Delta m_{EMI-BF4}}{\Delta t_{operation}} \tag{3}$$

$$I_{sp}^{average} = \frac{1}{g_0}\frac{F_{measured}\Delta t_{operation}}{\Delta m_{EMI-BF4}} \tag{4}$$

$$\eta_{total}^{average} = \frac{{F_{measured}}^2}{2\dot{m}_{average}P_{el}} \tag{5}$$

With the measured propellant mass-loss of $\Delta m_{EMI\text{-}BF4}$=8.6 mg for the thruster firing time $\Delta t_{operation}$=110 min, we get an average mass flow-rate of $1.303 \cdot 10^{-9}$ kg/s with Eq. (2).

By calculating the factor ($F_{measured}$ $\Delta t_{operation}$) for every emission current value in Fig. 12 and dividing it by the total mass loss $\Delta m_{EMI\text{-}BF4}$, we get a direct I_{sp} result of 439.75 s according to Eq. (3), which is an average over the entire current range as well. Instead of using the average mass flow-rate from before, we calculated the FΔt-factor for each current value which gives more weight to longer operating times of distinct current levels throughout the tests.

Regarding total efficiency, we employ equal experimental values used so far. At an exemplary force of (8.32 ± 0.27) µN with a power supply current of 100 µA and a voltage of 842 V, which results in an electrical power of P_{el}=0.0842 W, we get a total efficiency of 31.5% with Eq. (5). We neglect error calculation at this point, since these values are averaged and do not reflect distinct operating regimes in the first place. However, specific impulse and efficiency calculations for electrospray thrusters remain challenging, since theoretical calculations and experimental data deviate significantly in literature. There is a major discrepancy in thruster efficiency between theoretical predictions (80–91%) [30] and actual efficiencies from experiments (24–60%) [30], which is not yet fully understood, but also reflected in I_{sp}-values. Natisin et al. [15], for example, investigated this phenomenon with 1-ethyl-3-methylimidazoliumtetrafluoroborate (EMI-BF4) by comparing data from time of flight (ToF) measurements, which is an indirect I_{sp}-determination method, to the direct method of comparing thruster weight before and after a distinct emission duration. Their observation resulted in a large discrepancy in specific impulse of 3831 s (ToF-method) and 1440 s (weighing-method), which implies the presence additional neutral-particle related effects in electrospray thrusters, that are only detectable with direct measurements, since indirect methods like ToF or retarding potential analyzers (RPAs) only detect charged constituents in the expelled plume. This "anomalous" mass-loss phenomenon has profound implications for the use of electrospray thrusters and further clarification demands high-resolution direct measurements of thrust and mass-loss, which is well within the capability of our thrust balance and represents our next goal after iterating the collector setup.

After the room-temperature characterization of thrust for EMI-BF_4, we heated the device for several hours to elevate temperatures on the emitters. After several hours with a heater temperature of 100 °C, the thermocouples close to the emitter array showed a temperature of 43 °C at the PEEK mount. We assumed comparable temperatures at the emitters, but direct temperature detection at the emitter interface was not possible to prevent short-circuits.

Figure 14 (left) represents a direct comparison of thrust versus emitter current from 50 μA to 200 μA. At first, we observe equal behavior as before with the negative polarity exerting slightly more thrust than the positive polarity. This observation persists even at the data points with increased temperature. In general, we obtain slightly higher thrust values for a given amount of emitter current at higher temperatures. The viscosity decrease may support heavier ion species to leave the meniscus, hence larger thrust values for a given amount of current, as indicated in TOF measurements at different viscosities by Lozano et al. [24].

Furthermore, Fig. 14 (right) displays the effects of temperature change on emitted current. Here, each data point is obtained through operational parameters during consecutive thrust measurements from Fig. 14 (left). At a temperature of 28 °C and a PSU current of 80 μA, the starting voltage required 858 V. After heating the device to 43 °C, the starting voltage for a commanded 80 μA resulted in 835 V, which is considerably lower.

Lozano et al. investigated the influence of temperature on viscosity for EMI-BF_4 and concluded, that a temperature increment from 25 °C to 50 °C leads to a viscosity decrement and, hence, the current increased by a factor of around two [24], which was confirmed in our experiments. The exemplary current increase of 60 μA in Fig. 14 (right) at 140 μA and 28 °C represents an increment factor of 1.43. When we assume a linear dependency of this factor from literature between 25 °C and 50 °C, we reach a factor of 1.43 at a temperature of 43 °C and it is therefore consistent with observations by Lozano

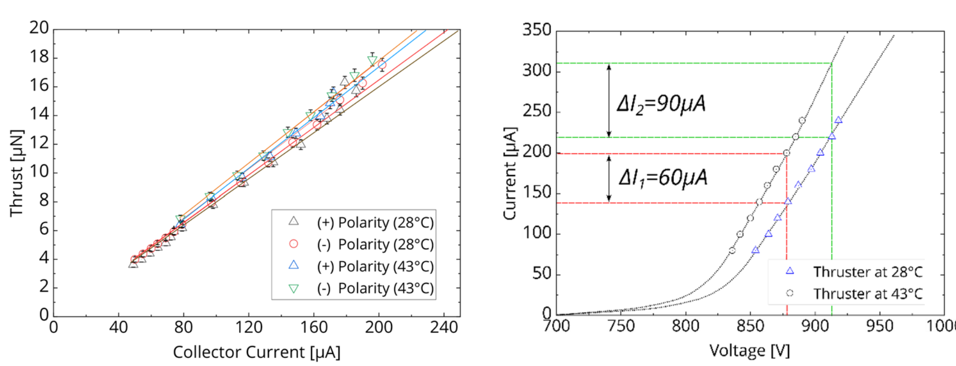

Fig. 14 Left: Comparison of thrust data for EMI-BF_4 at room-temperature (28 °C) and at 43 °C with both polarities for emission current between 50 μA and 200 μA. Each data point represents an average of 1–4 single measurements. Right: Visualized current increase for equal voltage levels due to a viscosity decrease from the elevated temperature operation

et al. This leads to the conclusion, that the temperature at the emitter was most likely 43 °C, as indicated by the thermocouples next to the emitters due to many hours of heating. We see an equal situation at higher currents, when comparing the commanded current of 220 μA at 28 °C and the extrapolated current increment to 315 μA at 43 °C, which results in a factor of 1.43 as well. In conclusion, the emitted current increment from temperature impact is consistent within the measured range and temperatures at the array. In future experiments we plan to increase the temperature further with an advanced thruster mounting and better heat conduction from the heater to the arrays. The thruster's total operating time throughout all tests accumulated to 232.6 min and it consumed 31.1 mg of EMI-BF_4 with visible residual depositions on the extractor in Fig. 15 (right) by comparing it to the newly assembled device (left).

EMI-Acetate

Throughout the entire measurement campaign, a second thrust device with a novel EMI-Acetate ionic liquid was positioned next to the thruster loaded with EMI-BF_4. It underwent equal heating periods and characterization attempts at emitter temperatures of 28 °C and 43 °C respectively.

Upon loading the device with EMI-Acetate, it was exposed to vacuum conditions and we performed a voltage sweep with equal voltage levels compared to EMI-BF_4 of up to 950 V. However, no emission was detected in this region. Further rise in voltage between 950 V and up to 1500 V is illustrated in Fig. 16 (left) for the positive polarity. First emission started at a voltage of 1100 V, reaching only 2.8 μA at 1500 V, which is drastically less compared to EMI-BF_4. Even less current was observed for same potentials at negative polarity in Fig. 16 (right) with only sub-μA at -1500 V. Although there was almost no extractor current detected, hinting at very good emitter-extractor-alignment, further potential increments to 2000 V could not extract significantly more current. Heating the device further deteriorated this trend by suppressing the emission entirely even when it was back at room temperature. Even loading the device with more propellant and checking all electrical connections did not change this behavior.

Upon inspecting the device immediately after venting the chamber, we noticed a bright spot on the array, as seen in Fig. 17. The bright spot arose from an absence of propellant within the central region which refilled on its own after several minutes. Disassembling

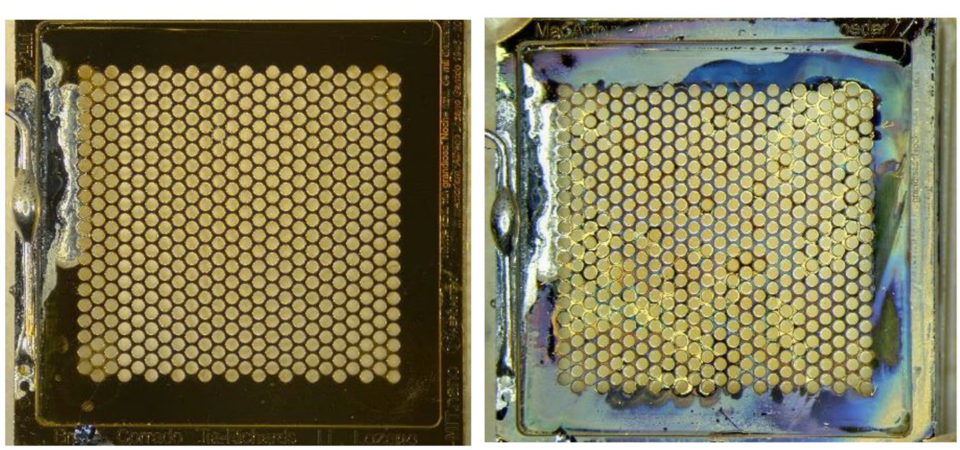

Fig. 15 Left: Newly assembled thrust device. Right: Depositions on the extractor grid after a total operating time of 232.6 min after consuming 31.1 mg of EMI-BF_4

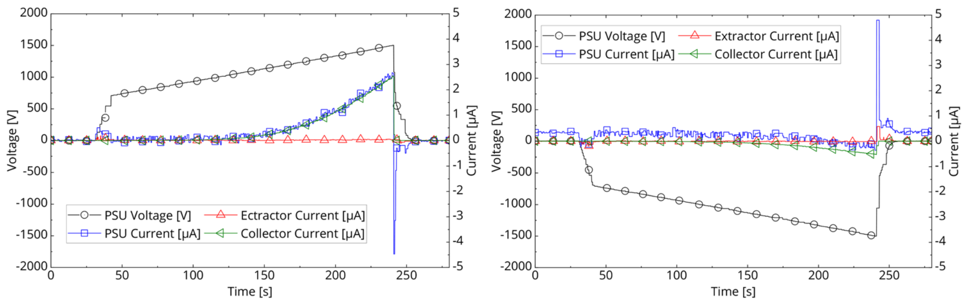

Fig. 16 Gradual voltage sweep at positive polarity with EMI-Acetate while observing emitted and intercepted current with a maximum current of 2.8 μA. Right: Gradual voltage sweep at negative polarity in the same manner

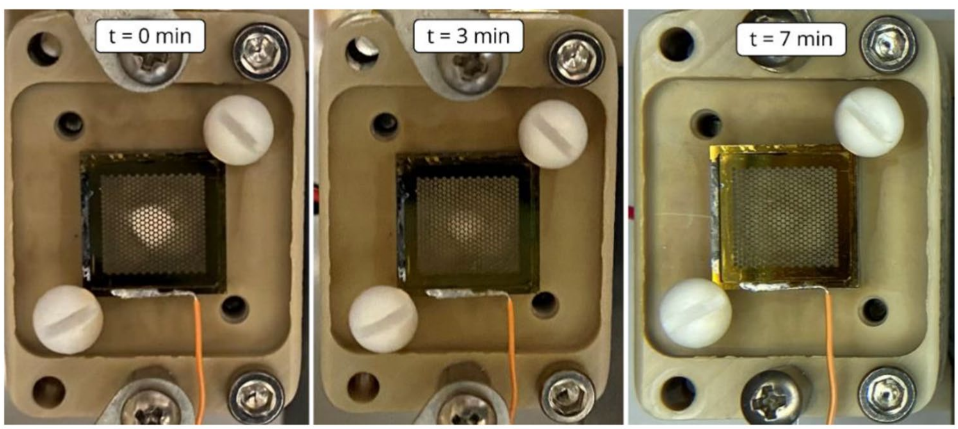

Fig. 17 Propellant anomaly with EMI-Acetate with the absence of propellant after venting the vacuum chamber (left). The void refilled on its own after several minutes

the device revealed a drastic viscosity increase of the ionic liquid. We detected a chemical incompatibility of the EMI-Acetate with storage materials (cellulose acetate filters) behind the emitter array, which clogged the porous array, effectively preventing any form of emission. Hence, the characterization of EMI-Acetate could not take place, yet. For future tests, we will implement different storage materials like fiberglass filters to prevent a dissolution of the ionic liquid.

Conclusion and outlook

Results obtained within the framework of this research demonstrate significant changes to the operating parameters of electrospray thrusters with EMI-BF_4 exposed to elevated temperatures. We demonstrated this with a dedicated measurement setup which included two electrospray devices mounted to a double-pendulum thrust balance with nanonewton resolution. The array's temperature was increased to 43 °C by an on-board heater and kept for several hours to ensure steady-state temperatures throughout each component and the ionic liquid. All results were compared to room-temperature data at 28 °C and indicated a drastic viscosity decrease which increased emitted current by a factor of 1.43 for equal voltage levels between these temperatures. Thrust values resulted in a difference of 3% between the maximum (43 °C) and minimum (28 °C) temperature, which was independent of the emission current.

Furthermore, thrust data at room-temperature revealed a difference between positive and negative polarity with slightly higher values for the latter. This was unexpected as the ion masses for EMI^+ and BF_4^- differ at the pure ion regime in favor of the cation, which would lead to slightly increased thrust for the positive polarity. We attribute this to a different operating regime induced by a marginal misalignment between emitter and extractor array as well as close distances to the collector, but this has to be investigated further with plume diagnostics like TOF. However, the thrust difference between both polarities persisted even at elevated temperatures. In future measurements we replace the collector with a much larger collector that fills the vacuum chamber almost completely instead of locally around the thrust device. In summary, the thruster with EMI-BF_4 was operated for 232.6 min and it consumed 31.1 mg of ionic liquid (EMI-BF_4). Regarding specific impulse we calculated an ideal I_{sp} of 1044 s utilizing the calculated charge to mass ratio of 58.9 C/g at exemplary voltage levels. By calculating the factor ($F_{measured}$ $\Delta t_{operation}$) for each emission current and dividing it by the total mass loss, we obtained a direct I_{sp} result of 439.75 s and a total efficiency of 31.5% at an electrical power of 0.0842 W. However, it is important to mention that these values are averaged over the entire emission current range instead of a single localized current and voltage level. Using this assumption, the calculated values will not be applicable to distinct emission states.

Initial data for the EMI-Acetate ionic liquid revealed a chemical incompatibility between the liquid and filter materials in the storage assembly, which prevented emission entirely. Hence, these tests will be repeated with more suitable materials in the future.

With the obtained thrust noise of sub-nN even single emitters instead of entire arrays may be characterized in future test campaigns to further contribute to the development and investigation of electrospray thrusters.

Nomenclature

$F_{measured}$	Measured Thrust
g_0	Gravitational constant
I_{sp}	Specific impulse
m	Ion mass
$\dot{m}_{average}$	Average propellant mass flow rate
η_{total}	Total thruster efficiency
$\Delta m_{EMI-BF4}$	Measured propellant mass loss
P_{el}	Electrical power
q	Ion charge
$\Delta t_{operation}$	Thruster's operational time
$U_{emitter}$	Emitter voltage

Acknowledgements
We would like to thank Ximo Gallud, Mia Bruno and Matt Corrado from MIT's Space Propulsion Laboratory for preparing the emitter and extractor arrays, synthesizing the ionic liquids and providing assistance for the thruster assembly at the TUD laboratory.

Author contributions
Development of the measurement infrastructure: [O. Neunzig, M. Tajmar], Development of the Electrospray System: [P. Lozano], Methodology: [O. Neunzig, M. Tajmar, P. Lozano], Analysis and investigation: [O. Neunzig, P. Lozano], Visualization [O. Neunzig]; Writing (original draft preparation): [O. Neunzig]; Writing (review and editing): [O. Neunzig, M. Tajmar, P. Lozano], Resources: [M. Tajmar, O. Neunzig, P. Lozano], Supervision: [M. Tajmar, P. Lozano]. All authors have read and agreed to the submitted version of the manuscript.

Funding
Open Access funding enabled and organized by Projekt DEAL. Open Access funding enabled and organized by Projekt DEAL. Not applicable.

Data availability
Data sets are available from the corresponding author on request.

Declarations

Competing interests

The authors declare no competing interests.

Received: 31 December 2024 / Accepted: 8 June 2025

Published online: 23 June 2025

References

1. Cidoncha XG, Lozano PC, Bendimerad P, Petro EM, Hampl SK (2022) Modeling and Characterization of Electrospray Propellant-Surface Interactions, 2022 IEEE Aerospace Conference (AERO), Big Sky, MT, USA, pp. 1–11. https://doi.org/10.1109/AERO53065.2022.9843583
2. Elaine M, Petro X, Gallud SK, Hampl M, Schroeder C, Geiger, Paulo C, Lozano (2022) Multiscale modeling of electrospray ion emission. J Appl Phys 21 May 131(19):193301. https://doi.org/10.1063/5.0065615
3. Tajmar M, Neunzig O&, Weikert M (2022) High-accuracy thrust measurements of the emdrive and elimination of false-positive effects. CEAS Space J 14:31–44. https://doi.org/10.1007/s12567-021-00385-1
4. Kößling M, Tajmar M (2022) Design and performance of a nano-Newton torsion balance. Rev Sci Instrum 93:074502. https://doi.org/10.1063/5.0086975
5. Frieler T, Groll R (2018) A torsional sub-milli-Newton thrust balance based on a spring leaf strain gauge sensor. Rev Sci Instrum 075101. 89https://doi.org/10.1063/1.4996419
6. Hathaway G (2015) Sub-micro-Newton resolution thrust balance. Rev Sci Instrum. https://doi.org/10.1063/1.4933382. 86,105116
7. Polk JE, Pancotti A, Haag T, King S, Walker M, Blakely J, Ziemer J (2013) Recommended Practices in Thrust Measurements, 33rd International Electric Propulsion Conference, Washington DC, USA
8. Neunzig O, Weikert M, Tajmar M (2022) Thrust measurements and evaluation of asymmetric infrared laser resonators for space propulsion. CEAS Space J 14:45–62. https://doi.org/10.1007/s12567-021-0366-4
9. Neunzig O, Weikert M, Tajmar M (2022) Thrust measurements of microwave-, superconducting- and laser-type emdrives. Acta Astronaut 195:583–595. https://doi.org/10.1016/j.actaastro.2022.02.014
10. Neunzig O, Tajmar M, Schütt F, Möller M, Adelung R, Beisch H, Fiedler B (2022) Experimental Investigation of Passive Photon Propulsion with Aerographite. 8th Edition of the Space Propulsion Conference, Estoril, Portugal, SP2022_149
11. Krejci D, Mier-Hicks F, Thomas R, Haag T, Lozano PC (2017) Emission characteristics of passively fed electrospray Micro thrusters with propellant reservoirs. J Spacecr Rockets 54(2):447–458. https://doi.org/10.2514/1.A33531
12. Mier-Hicks F (2017) Spacecraft Charging and Attitude Control Characterization of Electrospray Thrusters on a Magnetically Levitated Testbed, Ph.D. thesis, Massachusetts Institute of Technology
13. Mier-Hicks F, Lozano PC (2015) Thrust Measurements of Ion Electrospray Thrusters using a CubeSat Compatible Magnetically Levitated Thrust Balance, 34th International Electric Propulsion Conference, Hyogo-Kobe, Japan
14. Krejci D, Mier-Hicks F, Fucetola C, Lozano P, Hsu A, Martel F (2015) Design and Characterization of a Scalable ion Electrospray Propulsion System., 30th International Electric Propulsion Conference, July 4–10, 2015, Hyogo-Kobe, Japan
15. Natisin MR, Zamora HL, Holley ZA, Arnold NI, McGehee WA, Holmes MR, Eckhardt D Efficiency mechanisms in Porous-Media electrospray thrusters. J Propul Power 2021 37:5, 650–659
16. Gilpin MR, McGehee WA, Arnold IN, Natisin MR, Holley ZA (2022) Dual-axis thrust stand for the direct characterization of electrospray performance. Rev Sci Instrum 1 June 93(6):065102. https://doi.org/10.1063/5.0087716
17. Lyne CT, Lium MF, Rovey J A brief review of diagnostics for electrospray propulsion, AIAA 2023– 0263. AIAA SCITECH 2023 Forum. January 2023.
18. Corrado MN, Wangari C, Finch MR, Parameswaran L, Cook M et al (2024) Performance Characterization of High-Density Electrospray Thrusters. 38th International Electric Propulsion Conference, Toulouse, France, June 23–28, 2024, IEPC-2024-811
19. De Saavedra B, Wijnen F, Correyero M, Arboleya S, G., and, Pérez D (2022) Direct Thrust Measurements of an Externally Wetted Electrospray Thruster. IEPC-2022-223
20. Courtney DG, Shea H, Dannenmayer K, Bulit A Charge neutralization and direct thrust measurements from bipolar pairs of ionic electrospray thrusters. J Spacecr Rockets 2018 55:1, 54–65
21. Haag TW (1997) Thrust stand for pulsed plasma thrusters. Rev Sci Instrum 1 May 68(5):2060–2067. https://doi.org/10.1063/1.1148097
22. Guo Y, Sun W, Sun Z, Wu Z, He J, Yang J, Wang N (2023) Direct thrust test and asymmetric performance of porous ionic liquid electrospray thruster. Chin J Aeronaut 36(4):120–133. https://doi.org/10.1016/j.cja.2022.09.007
23. Taylor G (1964) Disintegration of water drops in an electric field. Royal Soc Lond Proc Ser A 280:383–397
24. Lozano PC, Martínez-Sánchez M (2005) Ionic liquid ion sources: characterization of externally wetted emitters. J Colloid Interface Sci 282(2) Pages 415–421, ISSN 0021-9797. https://doi.org/10.1016/j.jcis.2004.08.132
25. Coffman C, Martínez-Sánchez M, Higuera F-J, Lozano PC (2016) Structure of the menisci of leaky dielectric liquids during electrically-assisted evaporation of ions. Appl Phys Lett 5 Dec 109(23):231602. https://doi.org/10.1063/1.4971778
26. Neunzig O, Tajmar M Verification of a Novel Collector-Thrust Measurement using Low-Power Hall-Effect Thruster, 9th Space Propulsion Conference, 20th-23rd May, 2024, ID: SP2024_318, Glasgow, Scotland
27. Gondol N, Drobny C, Neunzig O, Tajmar M (2019) Development and Characterization of a Miniature Hall-Effect Thruster Using Permanent Magnets. 36th International Electric Propulsion Conference, Vienna, Austria. IEPC-2019-634
28. Peter C, Tajmar M (2023) Development of a novel ambipolar plasma thruster for nanosatellites and air breathing applications, 74th international astronautical Congress (IAC), IAC-23, C4,8-B4.5A,2, x78195, Baku, Azerbaijan.
29. Tajmar M, Neunzig O, Weikert M (2022) High-accuracy thrust measurements of the emdrive and elimination of false-positive effects. CEAS Space J 14:31–44. https://doi.org/10.1007/s12567-021-00385-1
30. Uchizono NM, Marrese-Reading C, Arestie SM, Ziemer JK, Wirz RE (2021) The role of secondary species emission in vacuum facility effects for electrospray thrusters. J Appl Phys 14 Oct 130(14):143301

31. Klosterman MR, Rovey JL, Levin DA (2022) Ion-induced charge emission from unpolished surfaces bombarded by an [Emim][BF4] electrospray plume. J Appl Phys 28 June 131(24):243302
32. Hofheins GC, Ulibarri Z, Petro EM (2024) Electrospray Secondary Ion Mass Spectrometry Diagnostic– Design and Preliminary Results. IEPC-2024-666, Presented at the 38th International Electric Propulsion Conference, Toulouse, France, June 23–28
33. Geiger C, Hofheins G, Petro E Secondary species investigation of low energy electrospray plume impacts, 13 January 2025, PREPRINT (Version 1) available at Research Square [https://doi.org/10.21203/rs.3.rs-5742257/v1]
34. Fuller J, Carlin RT, Osteryoung RA (1997) The room temperature ionic liquid 1-Ethyl-3-methylimidazolium tetrafluoroborate: electrochemical couples and physical properties. J Electrochem Soc 144(3881). https://doi.org/10.1149/1.1838106

Publisher's note